JOURNAL OF SOLID STATE CHEMISTRY **122,** 444–447 (1996)
ARTICLE NO. 0140

LETTER TO THE EDITOR

Structural Phase Diagram of Perovskite $A_{0.7}A'_{0.3}MnO_3$ (A = La, Pr; A' = Ca, Sr, Ba): A New *Imma* Allotype

P. G. Radaelli,* M. Marezio,†,‡ H. Y. Hwang,‡,§ and S-W. Cheong‡

*Institut Max Von Laue–Paul Langevin, BP156, 38042 Grenoble Cedex 09, France; †Laboratoire de Cristallographie, CNRS/UJF, BP166, 38042 Grenoble Cedex 09, France; ‡AT&T Bell Laboratories, Murray Hill, New Jersey 07974; and §Joseph Henry Laboratory of Physics, Princeton University, Princeton, New Jersey 08544

Communicated by J. M. Honig, February 7, 1996

The structural phase diagram of $A_{1-x}A'_xMnO_3$ (A = La, Pr, Y, …; A' = Ca, Sr, Ba, …) as a function of the average A-site ionic radius $\langle r_A\rangle$ was determined from neutron powder diffraction data. In addition to the well-known *Pnma* and $R\bar{3}c$ phases, a new orthorhombic phase, with space group *Imma*, was found for large $\langle r_A\rangle$ at low temperatures. Refined structural parameters are reported for $La_{0.7}Ba_{0.3}MnO_3$ at 1.6 K (*Imma*) and at 293 K ($R\bar{3}c$). The *Imma* → $R\bar{3}c$ phase transition was studied as a function of temperature for the same $La_{0.7}Ba_{0.3}MnO_3$ sample, and determined to be first order.

Manganese oxide perovskites with the general formula $A_{1-x}A'_xMnO_3$ (A = La, Pr, Y, …; A' = Ca, Sr, Ba, …) have been the subject of renewed interest, due to the giant magnetoresistance (GMR) exhibited near the ferromagnetic (FM) ordering temperature T_C (1). In fact, for values of the electronic doping $x \sim 0.30$, the high-temperature paramagnetic state is electrically insulating, whereas the low-temperature FM state is metallic. T_C can be raised upon application of an external magnetic field, thereby producing the GMR effect. Very recently it has been shown that, at a constant value of the electronic doping level x, T_C can be tuned by changing the average radius $\langle r_A\rangle$ of the A-site ion (2, 3). It has also been shown that the peak value of the magnetoresistance is higher when T_C is lower, so that resistive changes of up to 11 orders of magnitude can be attained by applying a field of 5 T (2, 4). In the light of these results, we have undertaken an extensive study of the structural properties of $A_{1-x}A'_xMnO_3$ at constant electronic doping ($x = 0.30$), as a function of $\langle r_A\rangle$. The complete results of this study will be published elsewhere. In this letter, we describe the structural phase diagram of $A_{0.7}A'_{0.3}MnO_3$ as a function of $\langle r_A\rangle$. Three phases were found to exist in this phase diagram. Two of them, with space group *Pnma* and $R\bar{3}c$, were already known, while the third, with space group *Imma,* is a new structural allotype of $A_{1-x}A'_xMnO_3$. This new phase is present for large values of $\langle r_A\rangle$ at low temperature, and transforms into the well-known $R\bar{3}c$ phase with increasing temperature through a first-order transition.

The seven samples examined in this study were $Pr_{0.7}Ca_{0.3}MnO_3$, $La_{0.525}Pr_{0.175}Ca_{0.3}MnO_3$, $La_{0.7}Ca_{0.17}Sr_{0.13}MnO_3$, $La_{0.7}Ca_{0.13}Sr_{0.17}MnO_3$, $La_{0.7}Sr_{0.3}MnO_3$, $La_{0.7}Sr_{0.12}Ba_{0.18}MnO_3$, and $La_{0.7}Ba_{0.3}MnO_3$. The specimens were prepared by standard solid-state reaction in air (2). Oxygen was found to be stoichiometric by iodometric titration as well as from our refinements of neutron diffraction data. Therefore, the formal valence of manganese is equal to +3.3 for all these samples, corresponding to a formal Mn^{4+} content of 30%. Neutron powder diffraction data were collected with the D2B diffractometer of the Institute Laue–Langevin at various temperatures between 1.6 and 300 K in the high-intensity mode, using a wavelength of 1.594 Å. Structural parameters were refined by the Rietveld method, using the program GSAS. For each composition, $\langle r_A\rangle$ was calculated using the tabulated values of Ref. (5). All the samples examined are ferromagnetic at low temperatures, and those with $\langle r_A\rangle > 1.20$ Å are already ferromagnetic at room temperature. The sample with composition $Pr_{0.7}Ca_{0.3}MnO_3$ displays a very complex magnetic structure at low temperatures, with the existence of both ferromagnetism and antiferromagnetism. The AFM component of this structure has two propagation vectors ($\frac{1}{2}00$ and $\frac{1}{2}0\frac{1}{2}$), associated with two manganese sublattices (6). For all the other samples, a simple ferromagnetic model is sufficient to adequately describe the magnetic scattering. For these samples, the relatively low resolution of the low-angle data did not allow the direction of the moments to be determined (the differences in R factors between the various models being insignificant).

0022-4596/96 $18.00

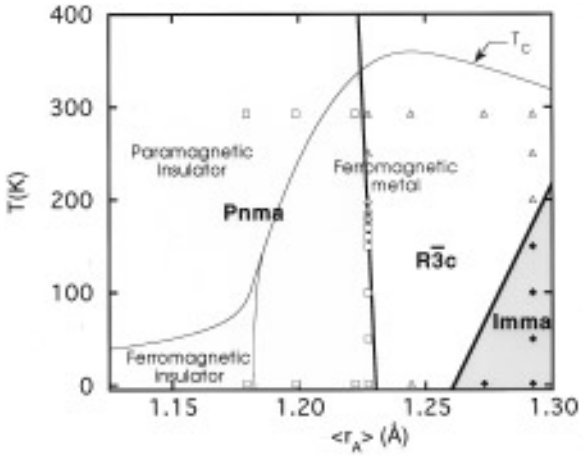

FIG. 1. Structural phase diagram of the $A_{1-x}A'_xMnO_3$ system (A = La, Pr; A' = Ca, Sr, Ba) as a function of $\langle r_A \rangle$. The three crystallographic phase regions are represented with different shadings and separated by thick lines. The T_C and metal–insulator transition curves (from Ref. (2)) are shown as thin lines. The neutron diffraction data sets of the present paper are shown as symbols (squares, *Pnma;* triangles, $R\bar{3}c$; diamonds, *Imma*).

The structural phase diagram, as determined from our neutron powder diffraction data, and the magnetic phase diagram replotted from Ref. (2) are shown in Fig. 1. At low $\langle r_A \rangle$, the samples were orthorhombic (i.e., $a \neq b \neq c$, $\alpha = \beta = \gamma = 90°$) at all temperatures. The orthorhombic lattice constants are related to the simple perovskite lattice parameter a_p by $a \approx c \approx \sqrt{2}a_p$ and $b \approx 2a_p$. The space group symmetry was *Pnma* (7). With increasing $\langle r_A \rangle$, a phase transition to a trigonal phase, with space group symmetry $R\bar{3}c$, occurs, both at room temperature and at 1.6 K, near $\langle r_A \rangle = 1.227$ Å. Urushibara *et al.* have evidence of a similar phase transition in a series of $La_{1-x}Sr_xMnO_3$ samples (8). Our $La_{0.7}Ca_{0.13}Sr_{0.17}MnO_3$ was trigonal at room temperature and orthorhombic at low temperatures, and underwent a first-order phase transition between the two structures at ~180 K. For larger values of $\langle r_A \rangle$, all samples were trigonal at room temperature. However, the two samples with larger $\langle r_A \rangle$ had orthorhombic symmetry at 1.6 K, with $a \approx c \approx \sqrt{2}a_p$ and $b \approx 2a_p$. The extinction rules for this low-temperature orthorhombic phase are consistent with a body-centered lattice. Due to the small value of the orthorhombic strain, it is rather difficult to determine whether other reflection conditions are present. However, based on Glazer's analysis of tilt distortions in pervoskites (9), the only orthorhombic body-centered space group with $a \approx c \approx \sqrt{2}a_p$ and $b \approx 2a_p$ is *Imma.* This space group was never previously found in the $AMnO_3$ system, and can be derived from the ideal perovskite structure by a single rotation of the octahedra around the [101] cubic direction. Therefore, further analyses of the low-temperature data in this part of the phase diagram were carried out in the *Imma* space group. The structural parameters for $La_{0.7}Ba_{0.3}MnO_3$ at 1.6 K (*Imma*) and 293 K ($R\bar{3}c$), as obtained from the Rietveld refinements of neutron powder diffraction data, are reported in Table 1. Selected bond distances and angles are listed in Table 2. Hexagonal axes were used for the $R\bar{3}c$ space group. Rietveld refinement profiles are shown in Fig. 2.

For $La_{0.7}Ba_{0.3}MnO_3$, additional data were obtained at

TABLE 1
Refined Structural Parameters of $La_{0.7}Ba_{0.3}MnO_3$ at 1.6 and 293 K

Parameter	T = 1.6 K	T = 293 K
Space group	*Imma*	$R\bar{3}c$
a (Å)	5.50888(8)	5.5378(1)
b (Å)	7.7882(1)	
c (Å)	5.53955(8)	13.5011(3)
V (Å^3)	237.669(6)	358.57(2)
La/Ba		
x	0	0
y	1/4	0
z	−0.0018(4)	1/4
U (Å^2)	0.0030(3)	0.0092(4)
Mn		
$x = y$	0	0
z	1/2	0
U (Å^2)	0.0021(5)	0.0037(5)
$M(\mu_B)$	3.33(3)	2.17(4)
O1		
x	1/2	0.4705(2)
y	1/4	0
z	0.0390(4)	1/4
n	1	0.989(6)
U_{11}(Å^2)	0.011(2)	0.0202(5)
U_{22}(Å^2)	0.004(2)	0.0133(6)
U_{33}(Å^2)	0.015(1)	0.0121(4)
U_{12}(Å^2)	0	0.0067(3)
U_{13}(Å^2)	0	−0.0022(3)
U_{23}(Å^2)	0	−0.0044(6)
O2		
x	1/4	
y	0.0195(2)	
z	3/4	
n	0.998(9)	
U_{11}(Å^2)	0.007(1)	
U_{22}(Å^2)	0.0139(7)	
U_{33}(Å^2)	0.0140(7)	
U_{13}(Å^2)	−0.0055(7)	
χ^2	2.462	2.716
R_{wp}	5.22%	5.44%

Note. Space group symmetries are *Imma* and $R\bar{3}c$, respectively. Numbers in parentheses are statistical errors of the last significant digit. The n values indicated for the oxygen atoms are refined fractional occupancies.

TABLE 2
Selected Bond Distances and Angles for $La_{0.7}Ba_{0.3}MnO_3$ at 1.6 and 293 K

Parameter	T = 1.6 K (*Imma*)			T = 293 K ($R\bar{3}c$)		
La/Ba–O (long) (Å)	*A*–O1	[×1]	2.976(3)	*A*–O	(×3)	2.932(1)
	A–O2[a]	[×2]	2.872(2)			
	A–O2[a]	[×2]	2.872(2)			
La/Ba–O (medium) (Å)	*A*–O1	[×2]	2.7637(3)	*A*–O	(×6)	2.76507(8)
	A–O2[b]	[×2]	2.648(2)			
La/Ba–O (short) (Å)	*A*–O2[b]	[×2]	2.648(2)	*A*–O	(×3)	2.606(1)
	A–O1	[×1]	2.564(3)			
Mn–O (Å)	Mn–O1	[×2]	1.9590(3)	Mn–O	(×6)	1.96166(9)
	Mn–O2	[×4]	1.9590(1)			
O–Mn–O (°)	O1–Mn–O2		89.94(8)	O–Mn–O		89.623(3)
Mn–O–Mn (°)	Mn–O1–Mn		167.3(1)	Mn–O–Mn		170.45(6)
	Mn–O2–Mn		171.10(9)			

Note. The grouping of the parameters emphasizes their reciprocal relationship in the two phases. Numbers in brackets are bond multiplicities. Numbers in parentheses are statistical errors of the last significant digit.
[a] Identical by symmetry.
[b] Identical by symmetry.

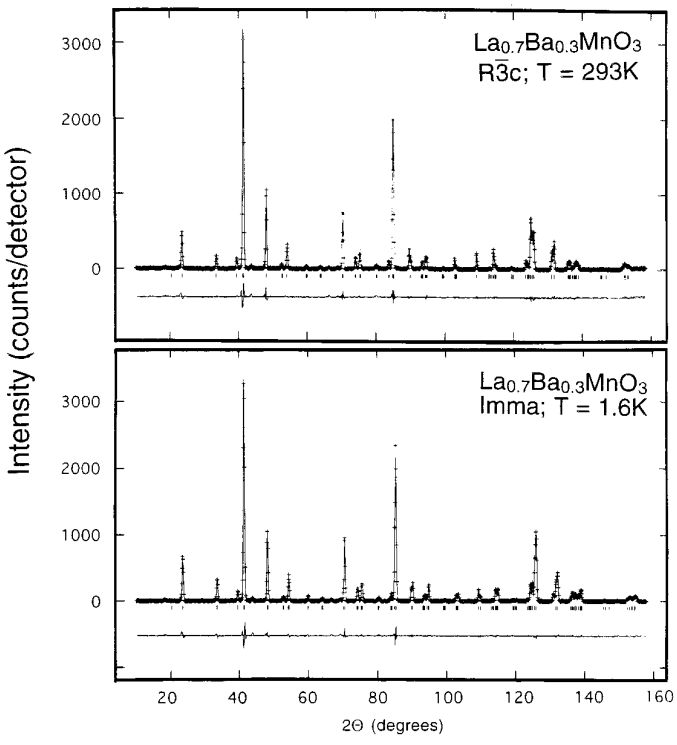

FIG. 2. Rietveld refinement profiles of neutron powder diffraction data for $La_{0.7}Ba_{0.3}MnO_3$ at 1.6 K (bottom) and 293 K (top). The plus (+) signs are raw data. The solid line is the calculated profile. Tick marks below the profile indicate the position of allowed Bragg reflections. The background was fit as part of the refinement, but subtracted before plotting. A difference curve (observed minus calculated) is plotted at the bottom.

50, 100, 150, 200, and 250 K, in order to determine the location and nature of the phase transition. The *Imma* → $R\bar{3}c$ phase transition could occur continuously only through an intermediate space group symmetry ($I2/a$). However, the sample was found to be trigonal at and above 200 K, and orthorhombic at and below 150 K, indicating that the phase transition is first order (a narrow monoclinic phase field between 150 and 200 K, although not impossible, is quite unlikely). Since both *Imma* and $R\bar{3}c$ are subgroups of $I2/a$, monoclinic axes appear to be the best choice to describe the phase transition. The geometric relationships between the orthorhombic and monoclinic cells are obvious, whereas the monoclinic unit vectors can be expressed in fractional coordinates of the trigonal cell (hexagonal axes) as

$$\mathbf{a}_M = \left[\frac{2}{3}, \frac{1}{3}, \frac{1}{3}\right]; \quad \mathbf{b}_M = \left[-\frac{4}{3}, -\frac{2}{3}, \frac{1}{3}\right]; \quad \mathbf{c}_M = [0, 1, 0].$$

It can be easily verified that $\mathbf{a}_M \perp \mathbf{c}_M$; $\mathbf{b}_M \perp \mathbf{c}_M$; $\gamma = \mathbf{a}_M \wedge \mathbf{b}_M \sim 90°$. The monoclinic lattice parameters a_M, b_M, c_M, and γ (unique axis: c) are related to the orthorhombic and trigonal parameters by the formulas

$$a_M = a_O; \quad b_M = b_O; \quad c_M = c_O; \quad \gamma = 90° \quad \text{(orthorhombic)}$$

$$a_M = \frac{1}{3}\sqrt{3a_T^2 + c_T^2}; \quad b_M = \frac{1}{3}\sqrt{12a_T^2 + c_T^2};$$

$$c_M = a_T; \quad \cos\gamma \frac{c_T^2 - 6a_T^2}{9a_M b_M} \quad \text{(trigonal).}$$

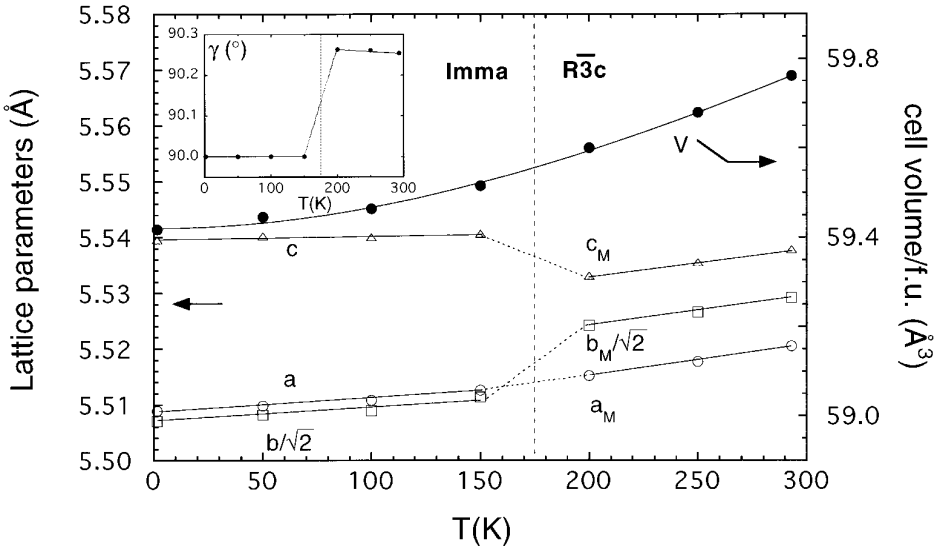

FIG. 3. Lattice parameters (open symbols) and cell volume/f.u. (closed circles) as a function of temperature for $La_{0.7}Ba_{0.3}MnO_3$. The cell volume/f.u. is obtained by dividing the unit cell volume by 4 and 6 for *Imma* and $R\bar{3}c$ (hexagonal setting), respectively. Monoclinic coordinates are used in the plot for the $R\bar{3}c$ phase (see text). The monoclinic angle γ is plotted in the inset. The vertical dashed line indicates the approximate position of the phase transition. Solid lines are drawn as guides (corresponding parameters in the two phases are connected with dotted lines). Error bars are smaller than the symbols.

The lattice parameters and unit cell volume/f.u. as a function of temperature for $La_{0.7}Ba_{0.3}MnO_3$ are shown in Fig. 3. The monoclinic angle γ is plotted in the inset. The discontinuous nature of the phase transition is evident in the lattice parameters, while the volume discontinuity, if present, appears to be rather small.

In summary, we have determined the structural phase diagram of $A_{0.7}A'_{0.3}MnO_3$ as a function of $\langle r_A \rangle$. In addition to the already known *Pnma* and $R\bar{3}c$ phases, a new orthorhombic phase with space group *Imma* was found for large $\langle r_A \rangle$ at low temperatures. Our findings of the structural richness of this system provides interesting implications for the understanding of its electronic and magnetic properties.

REFERENCES

1. R. von Helmolt, J. Wecker, B. Holzapfel, L. Schultz, and K. Samwer, *Phys. Rev. Lett.* **71,** 2331 (1993).
2. H. Y. Hwang, S-W. Cheong, P. G. Radaelli, M. Marezio, and B. Batlogg, *Phys. Rev. Lett.* **75,** 914 (1995).
3. R. Mahesh, R. Mahendiran, A. K. Raychaudhuri, and C. N. R. Rao, *J. Solid State Chem.* **120,** 204 (1995).
4. A. Maignan, C. Simon, V. Caignaert, and B. Raveau, unpublished (1995).
5. R. D. Shannon, *Acta Crystallogr. A* **32,** 751 (1976).
6. Z. Jirák, S. Krupicka, Z. Simsa, M. Dlouhá, and S. Vratislav, *J. Magn. Magn. Mater.* **53,** 153 (1985).
7. M. A. Gilleo, *Acta Crystallogr.* **10,** 161 (1957).
8. A. Urushibara, Y. Morimoto, T. Arima, A. Asamitsu, G. Kido, and Y. Tokura, *Phys. Rev. B* **51,** 14103 (1995).
9. A. M. Glazer, *Acta Crystallogr. A* **31,** 756 (1975).